Available online at www.sciencedirect.com
SCIENCE DIRECT
Journal of Catalysis 228 (2004) 433–446
JOURNAL OF CATALYSIS
www.elsevier.com/locate/jcat

Characterization and thiophene hydrodesulfurization activity of amorphous-silica–alumina-supported NiW catalysts

Y. van der Meer [a], E.J.M. Hensen [b,*], J.A.R. van Veen [b], A.M. van der Kraan [a]

[a] *Interfacultair Reactor Instituut, Delft University of Technology, Mekelweg 15, 2629 JB Delft, The Netherlands*
[b] *Schuit Institute of Catalysis, Eindhoven University of Technology, PO Box 513, 5600 MB Eindhoven, The Netherlands*

Received 22 July 2004; revised 15 September 2004; accepted 17 September 2004

Available online 28 October 2004

Abstract

The influence of the preparation method and sulfidation conditions on the structure and activity of ASA-supported NiW catalysts was investigated by a combination of ^{57}Co Mössbauer emission spectroscopy (MES), transmission electron microscopy (TEM), X-ray absorption spectroscopy (XAS), and thiophene hydrodesulfurization (HDS) activity measurements. Ni is sulfided already at low temperatures. This nickel sulfide phase redisperses at higher temperatures over the edges of WS_2 particles to form "Ni–W–S"-type phases. The formation of such highly active phases is facilitated by the partial transformation of intermediate WO_xS_y phases to WS_2 (W L_{III} edge XAS) at 673 K. In addition to this "Co–Mo–S" analogue nickel sulfide particles are present in dispersed form close to an oxysulfidic tungsten phase. It is found that the sulfidation of NiW/ASA closely resembles that of NiW/Al_2O_3. Trends in the HDS activity as a function of catalyst pretreatment were evaluated. A higher calcination temperature (from 673 to 823 K) decreases the HDS performance stemming from a lower W sulfidation degree and a more dominant presence of small oxysulfidic tungsten particles. Increasing the sulfidation pressure from atmospheric pressure to 15 bar leads to a strong increase of the HDS activity. Whereas sulfidation at 923 K results in a well-crystallized WS_2 phase (XAS), the concomitant loss in dispersion (TEM) is detrimental to its performance. Moreover, indications are found that more complete crystallization of the WS_2 phase results in a lower activity.

Keywords: Hydrodesulfurization; NiW; Amorphous silica–alumina; WS_2; Mössbauer emission spectroscopy; Extended X-ray absorption fine structure; Transmission electron microscopy

1. Introduction

More stringent environmental legislation has put pressure on oil refiners to improve the quality of product transportation fuels. Future fuel specifications necessitate active development work considering the improvement of processing technology and the introduction of new and more active catalysts. Specifically, the removal of alkylated dibenzothiophenes, the most refractory sulfur compounds in gas oil, needs to be addressed to arrive at low-sulfur transportation fuels. Recently, it has been demonstrated that alumina- and amorphous-silica–alumina (ASA)-supported sulfided NiW catalysts are promising for the conversion of alkylated DBT molecules at relatively low H_2S partial pressures [1,2]. The catalytic performance was found to be strongly dependent on the type of support and the reaction conditions [1,3]. For instance, whereas NiW/ASA was less active in the hydrodesulfurization (HDS) of 4-ethyl,6-methyldibenzothiophene compared to NiW/Al_2O_3 under H_2S-free conditions, NiW/ASA proved to be superior in the presence of 2000 ppm H_2S [1]. Numerous studies on the structure and performance of sulfided NiW/Al_2O_3 have been performed [1–17]. The sulfidation degree of tungsten appears to be crucial to the final catalytic HDS performance [2,4,8–12]. Clearly, the sulfidation behavior and catalytic properties of the promoted W- and Mo-based catalysts are different. NiW/Al_2O_3 is more difficult to sulfide than alumina-supported CoMo or NiMo [3,4]. This is mostly attributed to the formation of relatively strong

* Corresponding author. Fax: +31 40 245 5054.
E-mail address: e.j.m.hensen@tue.nl (E.J.M. Hensen).

0021-9517/$ – see front matter
doi:10.1016/j.jcat.2004.09.019

W–O–Al bonds [5], although it was alternatively put forward that the intrinsically strong W–O bonds make it difficult to fully sulfide tungsten oxides below 673 K [6]. Next to the presence of Co and Ni promoters [13] and additives as fluorine [14–16] or phophorus [17], the calcination temperature and the sulfidation temperature and pressure are the most important parameters influencing the final extent of tungsten sulfidation [3,8–12]. The mechanism of tungsten sulfidation has been studied by several research groups [4–17]. Breysse et al. [4] concluded that tungsten sulfidation to $W^{4+}S_2$ in alumina-supported NiW is rather limited at 673 K and that a significant fraction of tungsten may be present in higher oxidation states either as oxysulfides or as WS_3-like entities. Based on temperature-programmed sulfidation studies Reinhoudt et al. [2] have suggested WS_3 intermediates in the sulfidation of WO_3 to WS_2. Sun et al. [14] identified only very small amounts of WS_3-type phases as intermediates to tungsten disulfide in the sulfidation of NiW/Al_2O_3. On the other hand, detailed studies of the sulfidation of bulk tungsten oxides by Van der Vlies et al. [6] indicate that sulfidation of WO_3 proceeds via oxysulfide intermediates to WS_2. Sulfidation via WS_3-type phases appears to be unlikely. Oxysulfides intermediates have also been reported as very small particles on the alumina support at relatively low sulfidation temperatures [9–12]. Such particles show a good performance in liquid-phase DBT HDS but perform worse in gas-phase thiophene HDS [11,12]. A general trend for alumina-supported W catalysts is that a higher calcination temperature leads to a lower sulfidation degree at a given sulfidation temperature [11,12].

Concerning the role of promoters, Ni appears to be much more effective than Co and hence most research has been directed toward the NiW combination. Ni appears to be quite easy to sulfide [4,10,12,18]. This Ni-sulfide phase may be present as a separate Ni-sulfide phase or as small Ni-sulfide species that interact with WO_xS_y-type phases at relatively low sulfidation temperatures. At higher temperatures, the formation of WS_2 slabs results in the formation of "Ni–W–S"-type structures as observed by Mössbauer spectroscopy on ^{57}Co-doped NiW/Al_2O_3 [12]. This implies a redispersion of the Ni-sulfide phase to smaller, better ordered species [2,12]. We have recently focused on sulfided alumina- and carbon-supported NiW and CoW [12,19] and identified the "Ni–W–S" and "Co–W–S" analogues of "Co–Mo–S"-type phases by ^{57}Co Mössbauer spectroscopy. Additional indications for the decoration of the WS_2 edges by Ni species was provided by NO FTIR results of Reinhoudt et al. [10].

In view of the interesting catalytic properties of ASA-supported NiW, we further investigate the differences between alumina- and ASA-supported NiW catalysts here. Amorphous silica–alumina is a support material made up of γ-Al_2O_3 patches in an aluminosilicate matrix. We wish to address the relation between catalyst structure and HDS activity for ASA-supported NiW. The most important questions to be addressed are (i) how does the use of amorphous silica–alumina instead of alumina influence the sulfidation mechanism of the tungsten phase, (ii) does the redispersion of Ni observed for NiW/Al_2O_3 also take place in NiW/ASA, and (iii) why is the optimum Ni/W ratio generally higher than the optimum Co/Mo ratio. A fourth element of this study is the influence of the crystallinity of the WS_2 phase on the catalytic activity. Recently, we have found that complete sulfidation at 873 K of Mo in a $CoMo/Al_2O_3$ catalyst leads to a stronger decrease in HDS performance than is to be expected from the loss in dispersion [20]. This was attributed to a lower intrinsic activity of crystalline MoS_2 compared to fully sulfided but less ordered MoS_2.

The main characterization techniques include Mössbauer emission spectroscopy (MES) and extended X-ray absorption fine structure (EXAFS). MES was applied to follow the sulfidation of Ni species. To this end, Ni was doped with small amounts of ^{57}Co. This method was previously applied to study Ni(Mo) catalysts [21], zeolite-occluded Ni [22], and alumina- and carbon-supported NiW [12,19]. Crajé et al. [21] concluded that doping of Ni with ^{57}Co yields information on the various Ni phases present in sulfided Ni(Mo) catalysts. EXAFS was used to probe the local coordination environment of Ni and W during sulfidation. Information about morphology and dispersion was acquired by transmission electron microscopy (TEM). The catalytic activity was tested in atmospheric gas-phase thiophene HDS.

2. Experimental

2.1. Catalyst preparation

The ASA support, containing 60 wt% Al_2O_3 and 40 wt% SiO_2, was prepared by a cogelling procedure [23] and dried at 393 K overnight. Finally, the support was calcined in an air-circulation oven at 783 K for 5 h and at 949 K for an additional 2 h. The resulting ASA support consisted of bulk Al_2O_3 regions in a matrix of pure ASA. The pore volume of the ASA support was 0.67 ml g^{-1} with a particle size of 125–250 mm and a surface area of about 360 $m^2\,g^{-1}$.

NiW/ASA catalysts were prepared by pore-volume coimpregnation of a previously dried ASA support with an aqueous solution of ammonium metatungstate ($(NH_4)_6W_{12}O_{39} \cdot x H_2O$, Aldrich p.a.) and nickel nitrate ($Ni(NO_3)_2 \cdot 6H_2O$, Merck p.a.). The tungstate concentration was chosen such to result in final catalyst loadings of 15.2 wt%. Another sample was prepared by adding the W in the cogelling procedure of the preparation of the ASA support followed by pore-volume impregnation with an aqueous solution of nickel nitrate. This catalyst is denoted as NiW/ASA (W cogel). The catalyst for MES measurements was prepared by adding 60 MBq ^{57}Co as an aqueous solution of cobalt nitrate in 1 M HNO_3 (Cygne) to the impregnation solution, resulting in a ^{57}Co:Ni molar ratio of about 10^{-4}:1. This catalyst is denoted as ^{57}Co:NiW/ASA.

The resulting materials were dried in static air at 383 K overnight and subsequently calcined at temperatures of 673,

773, or 823 K in air-circulation oven for 2 h. The various catalysts are denoted by their calcination temperature, i.e., NiW/ASA-673, NiW/ASA-773, or NiW/ASA-823. NiW/ASA-773 (W cogel) was calcined at 723 K, while NiW/ASA-383 was only dried at 383 K.

One catalyst was specifically prepared for EXAFS measurements. This material has a Ni/W atomic ratio of 0.60, a value chosen to increase the signal-to-noise ratio at the Ni *K* edge. In all other cases, the nickel nitrate concentration in the impregnation solution was chosen to arrive at a Ni/W atomic ratio of 0.25 at./at.

2.2. Mössbauer emission spectroscopy

A sample was placed in an in situ reactor, which has been described elsewhere [24]. All parts were made of stainless steel 316, thus allowing measurements in a H_2S/H_2 atmosphere. The reactor was placed horizontally so that the sample holder, a small cup of vespel (composite material, Du Pont), can be easily mounted.

MES spectra were recorded at ambient temperature using a constant-acceleration spectrometer in the triangular mode with a single-line $K_4Fe(CN)_6 \cdot 3H_2O$ absorber, which is enriched in ^{57}Fe. The velocity scale was calibrated with a ^{57}Co in Rh source and a SNP ($Na_2(Fe(CN)_5NO) \cdot 2H_2O$) absorber. Positive velocities correspond to the absorber moving away from the source and zero velocity corresponds to the peak position of the $K_4Fe(CN)_6 \cdot 3H_2O$ absorber measured with the ^{57}Co in Rh source. Spectra were fitted with calculated subspectra consisting of Lorentzian-shaped lines. Constituent peaks were constrained to have equal widths and equal integrated intensities.

2.3. Catalyst sulfidation

Prior to sulfidation, a MES spectrum of the fresh sample was recorded. Subsequently, samples were subjected to a stepwise sulfidation treatment in a 10 vol% H_2S in H_2 gas mixture at the following temperatures: 300, 373, 473, 573, 673 K. The sample was heated from room temperature to the sulfidation temperature in 1 h and kept at this temperature for an additional hour. After each sulfidation step, the sample was cooled to room temperature in the sulfidation mixture followed by recording the MES spectrum.

For comparison, a single-step sulfidation experiment was carried out by heating to 673 K at a rate of 6 K min^{-1} in a 10 vol% H_2S in H_2 gas mixture followed by an isothermal period of 2 h. After cooling to room temperature in the sulfiding mixture, the reactor was flushed with He for 15 min. The sulfided catalysts were stored in sealed glass ampoules via a recirculation-type glove box filled with Ar.

Catalysts are denoted as NiW/ASA-X (Y), where X refers to the calcination temperature and Y to the sulfidation temperature in Kelvin. NiW/ASA-823 (673) refers to a sample calcined at 823 K and stepwise sulfided to a temperature of 673 K. For the single-step sulfidation at a sulfidation temperature of 673 K, the catalyst is denoted as NiW/ASA-823 (s 673). While the majority of the catalysts were sulfided at a total pressure of 1 bar, NiW/ASA-823 (s 673, 15) represents a sample sulfided at a total pressure of 15 bar while maintaining the H_2S/H_2 ratio of 0.1.

2.4. Extended X-ray absorption fine structure

Catalyst samples were pressed in self-supporting pellets with an optimal thickness adjusted to have an absorption μx of about 2.5. High surface area graphite (Lonza HSAG-16) was mixed with the catalysts to produce a stable pellet. The pellets were mounted in an in situ EXAFS cell [25] and stepwise sulfided. The cell was closed after purging with He and transported to the beam line. After recording of the X-ray absorption spectra, the cell was reconnected to the gas system for the next sulfidation step.

Spectra were recorded at the Ni *K* edge and the W L_{III} edge. Data of the stepwise sulfidation series and of sulfided NiW/ASA (W cogel) sample were collected at the Swiss-Norwegian beam line (SNBL, BM1B) at the ESRF, Grenoble, France (storage ring 6.0 GeV, ring current 200 mA). Incoming X-rays were monochromated by a Si(111) channel-cut monochromator and a chromium-coated mirror was used for harmonic rejection. After positioning the cell in the beam, the sample was cooled to liquid N_2 temperature for successive EXAFS measurements at the Ni *K* edge and the W L_{III} edge. The rest of the data were measured at station 9.2 of the SRS, Daresbury, UK. This storage ring was operated at 2.0 GeV and the ring current was in the range of 180–250 mA. The Si(220) monochromator was detuned to 80% intensity to remove higher harmonics in the X-ray beam. Three scans were averaged before data analysis.

The XDAP program version 2.2.2 [26,27] was used for data treatment and analysis. The W–S and W–W coordination of WS_2 (Aldrich, 99%) measured at station 9.2 at the SRS, Daresbury, UK, were used as W–S and W–W reference. For the Ni–S reference the Co coordination in CoS_2 measured at station 8.1 at the SRS, Daresbury, UK, was taken. The use of a Co absorber instead of Ni is justified as the phases and backscattering amplitudes of neighboring elements such as Co and Ni hardly differ [28]. Other reference spectra were calculated with the FEFF code [29]. The k^3-weighted and k-weighted EXAFS functions were Fourier transformed (FT) and multiple shell fitting was performed in *R* space until a satisfactory fit was obtained for spectra in *R* space as well as in *k* space. The data were analyzed over the range $\Delta k = 2.5$–13.9 Å^{-1} for the Ni *K* edge and $\Delta k = 3.1$–18.4 Å^{-1} for the W L_{III} edge, while the ranges for the *R* fit were between 1.0 and 4.0 Å. The estimated accuracies of the EXAFS fit parameters were ±20% for the coordination number (N), ±0.04 Å for the coordination distance (R), ±20% for the Debye–Waller factor $\Delta\sigma^2$, and ±10% for the inner-potential correction ΔE_0.

2.5. Gas-phase thiophene hydrodesulfurization

Atmospheric pressure gas-phase thiophene HDS activity measurements were performed in a quartz microflow reactor. About 100 mg of catalyst was diluted with SiC (83 μm) to obtain a bed height of about 1.5 cm. After heating the catalyst at a rate of 6 K min^{-1} to 673 K in a 10 vol% H_2S in H_2 mixture and further sulfidation at 673 K for 2 h, the flow was switched to the reaction mixture. Thiophene vapor was obtained by passing H_2 through liquid C_4H_4S (Acros, > 99%) in a saturator equipped with a cooler, resulting in a mixture of 4 vol% thiophene in H_2. The reaction temperature was 673 K. The total gas flow was 50 ml min^{-1}. Products of the HDS reaction were analyzed by an online gas chromatograph (HP-5890, FID) equipped with a CP-Sil 5 CB column. The reaction rate coefficient k was calculated assuming first-order kinetics in thiophene.

2.6. Transmission electron microscopy

Transmission electron microscopy was performed at the National Center for High Resolution Electron Microscopy at the Delft University of Technology, Delft. TEM micrographs were obtained by a Philips CM 30 T electron microscope operated at 300 kV with a LaB_6 filament as the source of electrons [30]. Samples were prepared by mounting a few droplets of a suspension of ground sulfided catalyst in ethanol on a Quantifoil microgrid carbon polymer supported on a copper grid followed by drying under ambient conditions, all in an Ar-flushed glove box. Samples were transferred to the microscope in a special vacuum-transfer sample holder. EDX elemental analysis was performed using a LINK EDX system. At least 10 micrographs for each sample were taken with a magnification of 490,000. The number of visible WS_2 stacks, the average number of layers per stack (stacking degree), and the average slab length were determined by manual inspection of at least 3 representative micrographs.

3. Results

3.1. Mössbauer emission spectroscopy

MES spectra for ^{57}Co:NiW/ASA-383 after stepwise sulfidation up to 673 K are presented in Fig. 1. The spectral shape clearly changes with increasing sulfidation temperature, most notably upon sulfidation above 473 K. The fit parameters are collected in Table 1. In the freshly prepared state, the sample predominantly contains ^{57}Co:Ni-oxide species with a spectral contribution (A) of 82%, while the remainder is made up by high-spin 2+ species with a quadrupole splitting (QS) of 2.39 mm s^{-1}. This high-spin 2+ state can be attributed to oxidic ^{57}Co:Ni species [31] which represent nickel atoms in close contact with the W phase or the ASA support. The spectral contribution of this

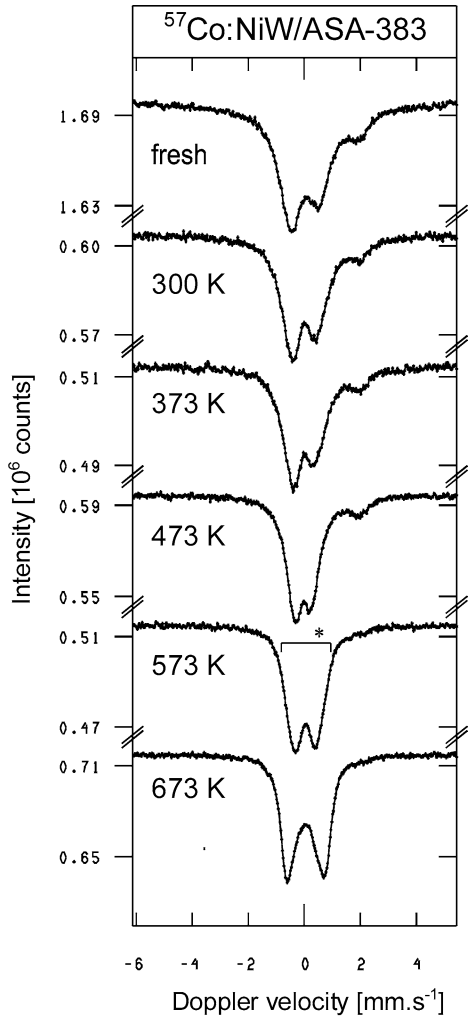

Fig. 1. MES spectra of ^{57}Co:NiW/ASA-383, fresh and sulfided at indicated temperatures, showing ^{57}Co:"Ni–W–S" formation (indicated with ∗) at 573 K.

state remains fairly constant with increasing sulfidation temperatures up to 473 K. Besides the high-spin 2+ component, a second contribution (QS = 0.93 mm s^{-1}) is present after sulfidation at 300 K, which is due to (partly) sulfided ^{57}Co:Ni. The QS of this species decreases to 0.61 mm s^{-1} after sulfidation at 473 K. A decreasing QS reflects the growth and/or ordering of initially highly dispersed Co-sulfide particles [31,32] in CoMo-based catalysts. Similar trends for the present ^{57}Co-probed Ni catalysts are taken as an indication of the evolution of small Ni-(oxy)sulfide particles to larger and/or better ordered ones with increasing sulfidation temperature. Concomitant with the decrease of the spectral contribution of the high-spin 2+ component at a sulfidation temperature of 573 K, a new contribution appears with an isomer shift (IS) of 0.29 mm s^{-1} and a QS of 1.24 mm s^{-1}. In the absence of W, this doublet was not observed [21,22]. From the similarity of the Mössbauer fit parameters for this phase to the one observed for Co–Mo–S-type phases, we assign this doublet to a ^{57}Co:Ni–W–S-type phase. The spectral contribution of this phase increases to

Table 1
MES parameters of ^{57}Co:NiW/ASA-383 after successive sulfidation steps

	^{57}Co:Ni-oxide				High spin 2+				^{57}Co:Ni-(oxy)sulfide				^{57}Co:"Ni–W–S"			
	IS (mm s^{-1})	QS (mm s^{-1})	Γ (mm s^{-1})	A (%)	IS (mm s^{-1})	QS (mm s^{-1})	Γ (mm s^{-1})	A (%)	IS (mm s^{-1})	QS (mm s^{-1})	Γ (mm s^{-1})	A (%)	IS (mm s^{-1})	QS (mm s^{-1})	Γ (mm s^{-1})	A (%)
Fresh	0.23	1.04	1.07	82	0.99	2.39	0.74	18								
300					1.03	2.38	0.58	13	0.22	0.93	0.92	87				
373					1.04	2.36	0.54	14	0.21	0.85	0.90	86				
473					1.03	2.29	0.71	16	0.19	0.61	0.70	84				
573					0.99	2.58	0.50	3	0.27	0.66	0.64	77	0.29	1.24	0.49	20
673									0.28	0.79	0.71	52	0.28	1.41	0.45	48

Isomer shift, IS ± 0.03 mm s^{-1}; quadrupole splitting, QS ± 0.03 mm s^{-1}; linewidth, Γ ± 0.05 mm s^{-1}; spectral contribution, A ± 5%.

48% after sulfidation at 673 K. At the same time, the contribution of the Ni-sulfide phase decreases with an additional increase of the QS. We take this as a strong indication that part of the Ni-(oxy)sulfide particles redisperses resulting in formation of Ni–W–S-type phases. The observation of an increase of the quadrupole splitting of the Ni-(oxy)sulfide phases can be reconciled by noting that the Ni-(oxy)sulfide particles become smaller and/or more disordered [21,22].

3.2. W EXAFS

The W EXAFS k^3-weighted FT functions of stepwise sulfided NiW/ASA-673 are given in Fig. 2. After sulfidation at relatively low temperatures, two W–O contributions are visible with oxygen atoms at radial distances of 1.73 and 1.99 Å. These interatomic distances correspond to the W–O distances in the first coordination shell of WO_3 [33,34]. After sulfidation at 573 K, tungsten is partially sulfided as is apparent from the small W–S contribution with $R_{W–S} = 2.42$ Å and $N_{W–S} = 0.4$ (fit results not included in Table 2). No evidence for intermediate WS_3-like species was found. After sulfidation at 673 K, the spectrum consists of two main contributions, a W–S contribution at a distance 2.40 Å and a W–W coordination at 3.15 Å. This clearly points to the dominant presence of WS_2. On the other hand, the value of $N_{W–S}$ of 4.4 is rather low and may point to incomplete sulfidation at this stage. We suspect that there remains some oxygen in the tungsten sulfide structures and strictly speaking the resulting phase should be denoted oxysulfidic. The remaining catalysts were studied after single-step sulfidation. The k^3-weighted FT functions of the single-step sulfided catalysts are presented in Figs. 3a and b. The fit results for NiW/ASA-673 (s 923) in Table 3 show that the W–S and W–W coordination numbers are close to 6. These values agree with those for bulk WS_2. The presence of a second coordination

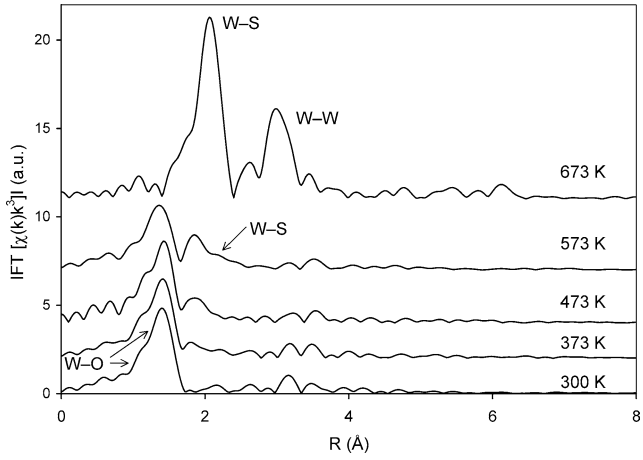

Fig. 2. k^3-weighted W EXAFS FT functions of NiW/ASA-673 after stepwise sulfidation at indicated temperatures. Tungsten sulfidation starts at 573 K as derived from the corresponding fit results in Table 2.

Table 2
W L_{III} edge EXAFS parameters of selected NiW/ASA catalysts after single-step and stepwise sulfidation

Catalyst	W–O (1)				W–O (2)				W–S				W–W			
	N	R (Å)	$\Delta\sigma^2 \times 10^{-3}$ (Å^2)	ΔE_0 (eV)	N	R (Å)	$\Delta\sigma^2 \times 10^{-3}$ (Å^2)	ΔE_0 (eV)	N	R (Å)	$\Delta\sigma^2 \times 10^{-3}$ (Å^2)	ΔE_0 (eV)	N	R (Å)	$\Delta\sigma^2 \times 10^{-3}$ (Å^2)	ΔE_0 (eV)
NiW/ASA-673 (s 673)	–	–	–	–	–	–	–	–	4.4	2.40	1.2	−2.3	2.8	3.15	2.2	−3.4
NiW/ASA-673 (s 923)	–	–	–	–	–	–	–	–	6.8	2.41	0.4	−0.3	5.3	3.16	0.0	−0.8
NiW/ASA-773 (s 673)	–	–	–	–	–	–	–	–	5.6	2.41	0.6	−1.5	3.6	3.16	0.3	−2.6
NiW/ASA-773 (s 673, 15)	–	–	–	–	–	–	–	–	6.1	2.42	0.6	−1.4	4.0	3.17	0.2	−1.4
NiW/ASA-823 (s 673, 15)	–	–	–	–	–	–	–	–	4.8	2.41	1.3	−0.2	2.8	3.17	1.2	−4.2
NiW/ASA-823 (s 573)	5.3	1.73	14	−19	2.1	1.99	2.1	2.4	1.8	2.39	3.0	1.7	1.0	2.75	3.8	6.7
NiW/ASA-723 (W cogel) (s 673)[a]	1.9	1.72	4.9	20	2.1	1.94	0.6	20	3.6	2.40	0.7	−0.2	2.8	3.15	1.9	−2.3

Estimated accuracies: N ± 20%, R ± 0.04 Å, $\Delta\sigma^2$ (Å^2) ± 20%, ΔE_0 (eV) ± 10%; –, contribution not present; W–O (1) is the first W–O coordination present, W–O (2) is the second W–O coordination present; catalyst notation is explained in the text.

[a] Second W–W contribution present: $N = 0.4$, $R = 2.72$ Å, $\Delta\sigma^2 = 0.0$ Å^2, $\Delta E_0 = 19$ eV.

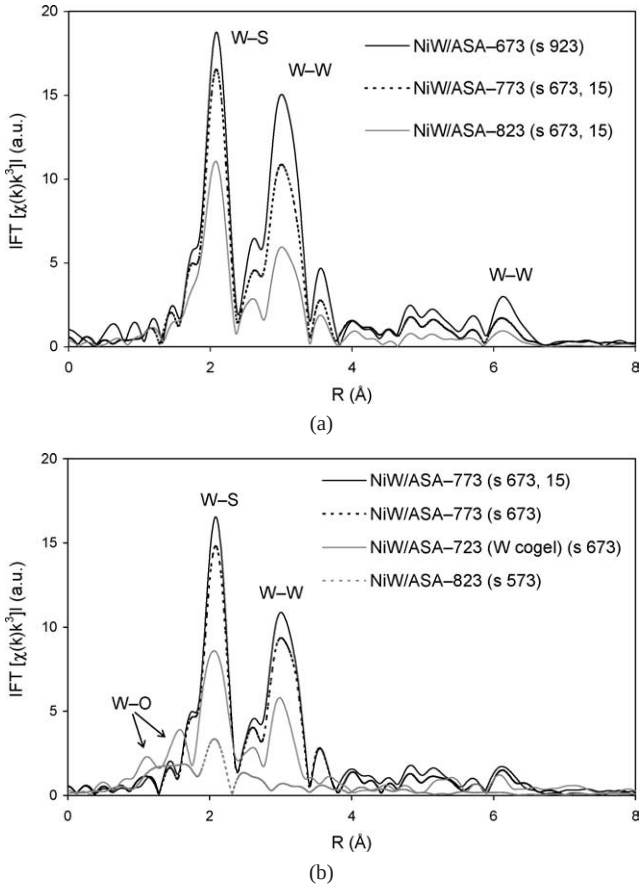

Fig. 3. W EXAFS k^3-weighted FT functions of selected NiW/ASA catalysts: (a) NiW/ASA-823 (s 673, 15), NiW/ASA-773 (s 673, 15), and NiW-673 (s 923) and (b) NiW/ASA-823 (s 573), NiW/ASA-723 (W-cogel) (s 673), NiW/ASA-773 (s 673), and NiW/ASA-773 (s 673, 15). The corresponding fit parameters are collected in Table 3. A second coordination shell at radial distances larger than 4 Å is visible in almost all spectra (indicated in Fig. 3a).

shell at radial distances larger than 4 Å suggests a relatively crystalline WS_2 phase for this high sulfidation temperature. NiW/ASA-773 (s 673) displays a WS_2-like structure with $N_{W–S} = 5.6$, which indicates nearly complete W coordination by sulfur. Increasing the sulfidation pressure from 1 to 15 bar leads to an increase of $N_{W–S}$ from 5.6 to 6.1 and an increase of $N_{W–W}$ from 3.6 to 4.0. This can be easily observed in Fig. 3b as an increase in the intensities of the corresponding features. The W–W coordination numbers of 3.6 and 4.0, respectively, are considerably lower than 6. These values are typical for small supported MeS_2 (Me = Mo, W) particles, although the effect of structural disorder also must be taken into account [35].

The influence of increasing the calcination temperature from 773 to 823 K can be evaluated from a comparison between NiW/ASA-773 and NiW/ASA-823 after a similar sulfidation treatment, i.e., sulfidation at 673 K and 15 bar. Table 2 gives the corresponding W–S and W–W coordination numbers. Clearly, the values for these coordination numbers are significantly lower for NiW/ASA-823. Thus, an increase of the calcination temperature leads to a decrease of the sulfidation degree. Finally, the spectra of NiW/ASA-823 (s 573) and NiW/ASA-723 (W cogel) (s 673) are different from the other spectra in Fig. 3b. Here, we clearly observe two additional W–O contributions. These catalysts are thus partly oxidic, most likely due to the presence of WO_3 (see also Table 2). The cogel sample also contains features of a WS_2-type phase with $N_{W–S}$ of 3.6 and $N_{W–W}$ of 2.8, characteristic for incomplete WS_2 formation and the presence of some oxysulfidic particles. Compared with a similar catalyst prepared via the conventional route, i.e., NiW/ASA-773 (s 673), the sulfidation degree for NiW/ASA-723 (W cogel) is considerably lower, taking into account that the somewhat lower calcination temperature of the latter sample would induce the opposite effect. We thus attribute the lower sulfidation degree to differences in the preparation method. In short, the addition of W during preparation of the ASA support retards tungsten sulfidation.

NiW/ASA-823 (s 573) also exhibits a lower sulfidation degree with a value of 1.8 for $N_{W–S}$. The observed W–W distance of 2.75 Å agrees with $R_{W–W}$ in WS_3 ($R_{W–S} = 2.40$ Å, $N_{W–S} = 5$, $R_{W–W} = 2.75$ Å, $N_{W–W} = 2$) [36,37]. This phase can possibly be an intermediate one to the development of the WS_2 phase. After increasing the sulfidation to 673 K at a pressure of 15 bar, the transition to WS_2 formation has begun. We note that we only observed such an intermediate WS_3 phase for NiW/ASA-823.

3.3. Ni EXAFS

The k^3-weighted FT functions at the Ni K edge for stepwise sulfided NiW/ASA-673 are shown in Fig. 4. Table 3

Table 3
Ni K edge EXAFS parameters of NiW/ASA-673 after stepwise sulfidation

T_s (K)	Ni–O				Ni–S				Ni–Ni			
	N	R (Å)	$\Delta\sigma^2 \times 10^{-3}$ (Å^2)	ΔE_0 (eV)	N	R (Å)	$\Delta\sigma^2 \times 10^{-3}$ (Å^2)	ΔE_0 (eV)	N	R (Å)	$\Delta\sigma^2 \times 10^{-3}$ (Å^2)	ΔE_0 (eV)
300	6.1	2.01	7.4	6.7	0.5	2.22	1.2	1.2	0.9	3.04	4.1	−1.6
373	4.1	1.98	10	15	2.1	2.18	1.6	14	0.3	3.02	3.9	2.3
473	3.0	1.98	10	14	2.7	2.17	1.3	15	0.7	3.02	1.6	−0.2
573	2.2	1.94	6.1	14	2.7	2.19	0.2	12	0.8	2.98	1.4	7.4
673	–	–	–	–	5.6	2.22	3.4	0.0	–	–	–	–

Estimated accuracies: $N \pm 20\%$, $R \pm 0.04$ Å, $\Delta\sigma^2$ (Å^2) $\pm 20\%$, ΔE_0 (eV) $\pm 10\%$; –, contribution not present.

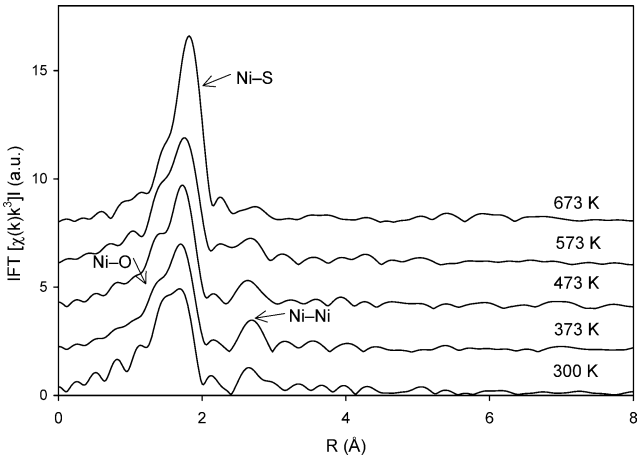

Fig. 4. k^3-Weighted Ni EXAFS FT functions of NiW/ASA-673 after stepwise sulfidation at various temperatures.

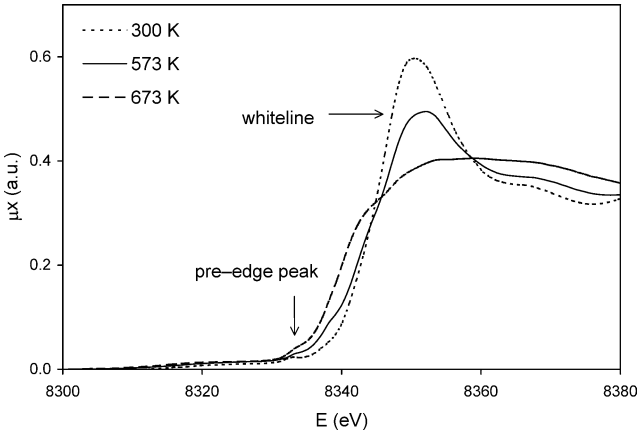

Fig. 5. XANES spectra at the Ni K edge of NiW/ASA-673 after sulfidation at various temperatures. Besides the differences in the whiteline and preedge peak, there is also a shift in edge position with increasing sulfidation temperature.

gives an overview of the multiple-shell-analysis fit parameters. Analysis of the spectrum for the room-temperature sulfided sample (300 K) indicates the presence of three contributions: a Ni–O contribution at a distance of 2.01 Å ($N_{\text{Ni–O}} = 6.1$), a Ni–S contribution at 2.22 Å ($N_{\text{Ni–S}} = 0.5$), and a Ni–Ni contribution at 3.04 Å ($N_{\text{Ni–Ni}} = 0.9$). These Ni–O and Ni–Ni distances approach the crystallographic distances in bulk NiO ($R_{\text{Ni–O}} = 2.08$ Å, $R_{\text{Ni–O}} = 2.96$ Å [37]). With increasing sulfidation temperatures, $N_{\text{Ni–O}}$ decreases in favor of an increasing value for $N_{\text{Ni–S}}$, demonstrating that Ni becomes progressively sulfided. Still, sulfidation is far from complete at 573 K. This is also visible in the XANES region displayed in Fig. 5, which presents the typical whiteline for a Ni–O interaction [38,39]. After increasing the sulfidation temperature to 673 K, the Ni–O and Ni–Ni contributions disappear. The whiteline also disappears due to the nonionic character of the Ni–S bond [40]. Moreover, we observe an increase of the preedge peak area around 8333 eV, characteristic for a 1s → 3d transition [41] and a shift of the edge position from 8347 to 8340 eV. The increase in the intensity of the preedge peak at a sulfidation temperature of 573 K is related to a change in local symmetry of Ni. The shift of the edge position to lower energy can be explained by a decrease of the valency of Ni. The value of $R_{\text{Ni–S}} = 2.21$ Å fits into the structural model of Ni–W–S as proposed by Louwers and Prins [42].

3.4. Transmission electron microscopy

The high-resolution TEM micrographs indicate an inhomogeneous distribution of the WS_2 slabs over different areas of the samples. EDX elemental analysis demonstrated that the WS_2 slabs are preferentially located on the alumina part of the ASA support, although slabs were also found in other parts of the support material. This tallies with the earlier finding that tungsten preferentially interacts with the alumina part of the support materials [7]. For each catalyst, we analyzed at least 550 WS_2-like slabs from three representative micrographs. The average slab lengths and stacking degrees of various sulfided catalysts are listed in Table 4. The corresponding slab length distributions and stacking degrees are shown in Fig. 6. As the slab length distribution was roughly similar for single-layered and multiple-layered slabs in the investigated samples, we report the slab length distribution for the total of slabs in a given catalyst. A detailed analysis of NiW/ASA-673 (s 673) indicates that the majority of slabs have a length in the range of 2–3 nm, while the average slab length amounts to 2.9 nm (see Table 4). The major fraction (∼ 70%) is present as single-layered slabs, leading to a relatively low stacking degree of 1.1. A small part of the sample contains a high slab density with multiple-stacked slabs, while the largest part of the sample consists of a lower density of slabs with mainly single and double layers (Fig. 7). Calcination at 773 K (NiW/ASA-773 (s 673)) instead of 673 K resulted in a decrease of the average slab length to 2.6 nm. The slab length distribution in Fig. 6a demonstrates that this decrease in average slab length is mainly caused by a higher fraction of very small

Table 4
Average slab length, average fraction of W at the edges, and average stacking degree in selected catalysts

Catalyst	Average slab length (nm)	Average fraction W(edge)[a]	Average stacking degree
NiW/ASA-673 (s 673, 1)	2.9	0.39	1.1
NiW/ASA-773 (s 673, 1)	2.6	0.43	1.4
NiW/ASA-773 (s 673, 15)	3.4	0.34	1.4
NiW/ASA-673 (s 923, 1)	4.4	0.27	1.5

[a] Derived from average slab length.

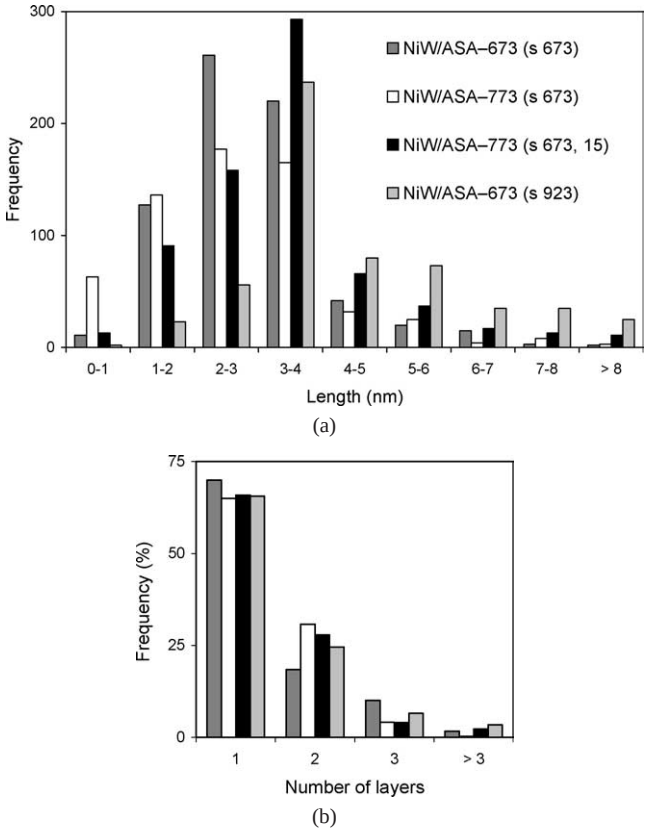

Fig. 6. Slab length distributions (a) and stacking degree (b) of three representative TEM micrographs of selected catalysts. The legend provided in (a) also applies to (b).

Fig. 7. TEM image of NiW/ASA-673 after sulfidation at 673 K showing single- and multiple-layered slabs representative for the largest part of the sample.

particles (< 1 nm), while the main part still has a length in the range of 2–3 nm. Furthermore, it is remarkable that calcination at 773 K also results in a higher stacking degree (from 1.1 to 1.4). Sulfidation of this catalyst at a pressure of 15 bar (NiW/ASA-773 (s 673, 15 bar)) results in the same stacking degree with a similar stacking distribution (Fig. 6b). However, clear changes are observed in the slab length distribution. A larger amount of slabs has a length of 3–4 nm leading to an average slab length to 3.4 nm. The slab length distribution of NiW/ASA-673 (s 923) in Fig. 6a also shows a maximum in the interval 3–4 nm. However, the average slab length of 4.4 nm is larger than in the previous sample due to a larger number of slabs with a length greater than 4 nm. The fraction of single-layered slabs is equal to that for the NiW/ASA-773 samples, although on average the multiple-stacked slabs have a somewhat higher stacking degree. The average stacking degree amounts to 1.5. Fig. 8 shows two representative TEM micrographs of NiW/ASA-673 (s 923).

3.5. Thiophene HDS activity

The thiophene HDS activities as a function of the Ni/W atomic ratio are plotted in Fig. 9. The activities are given per mole W and per mole Ni. The promotion effect of Ni on the activity per W atom is clearly observed. The activity sharply increases with increasing Ni/W atomic ratio up to a ratio of 0.60. At higher ratios, the activity levels off. At Ni/W atomic ratios below 0.40 at./at., the activity per Ni atom is more or less constant, but at higher ratios it declines somewhat. We take this as an indication that all available edge positions are occupied by Ni atoms and that excess Ni atoms cannot be accommodated on free WS_2 edges. This leads to a lower activity per Ni atom. Fig. 10 shows the relation between the thiophene HDS activity per mole W and the calcination temperature at a sulfidation temperature of 673 K. Increasing the calcination temperature from 673 to 823 K leads to a decrease of the activity. Moreover, an increase of sulfidation temperature from 673 to 923 K also results in a lower performance. An optimum thiophene HDS activity after sulfidation at 673 K was reported by Korányi et al. [43] for a sample similar to NiW/ASA-673. Here, we find a marked improvement in the HDS performance after an increase of the sulfidation pressure from 1 to 15 bar for a calcination temperature of 773 K and a sulfidation temperature of 673 K (Fig. 10).

4. Discussion

4.1. Influence of sulfidation temperature

The Ni EXAFS data show that already after sulfidation at 300 K part of the Ni oxide phase is sulfided in line with earlier results [4,10,12,18]. This is attributed to oxygen–sulfur

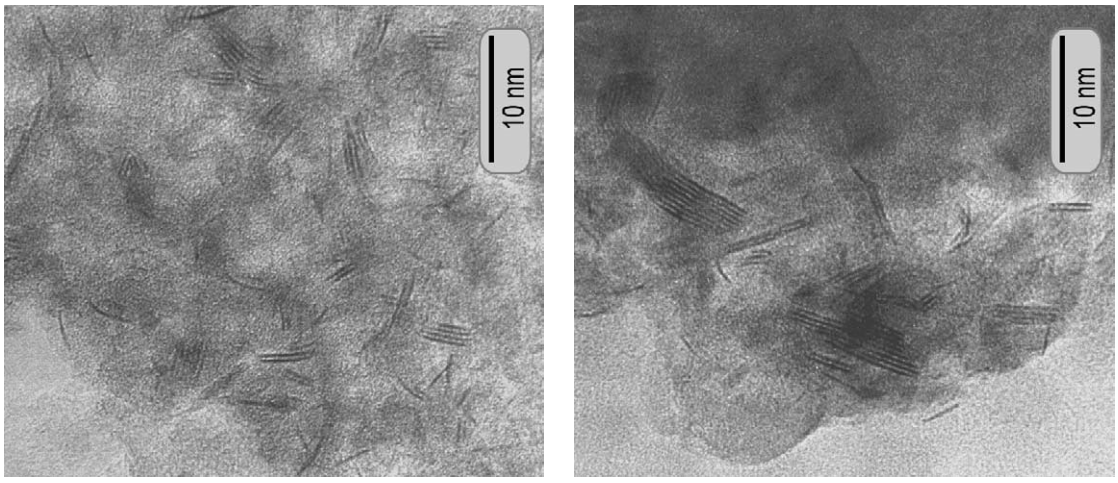

Fig. 8. TEM images of NiW/ASA-673 after sulfidation at 923 K showing that some parts contain up to eight WS_2 slabs (left), while other parts contain a variety of single and multiple stacked slabs (right).

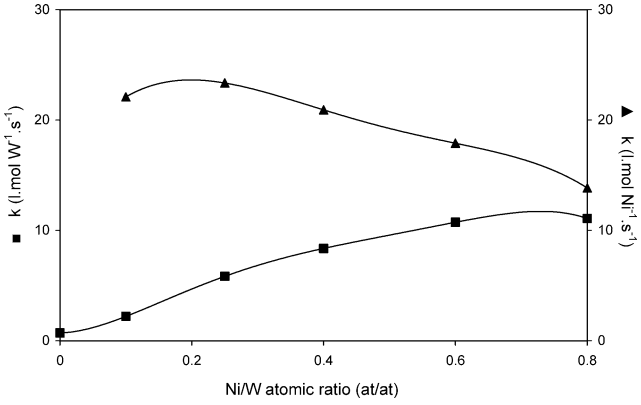

Fig. 9. Thiophene HDS activity of NiW/ASA-823 as a function of the Ni/W atomic ratio. The reaction rate constant k is given per mole W (■) and per mole Ni (▲).

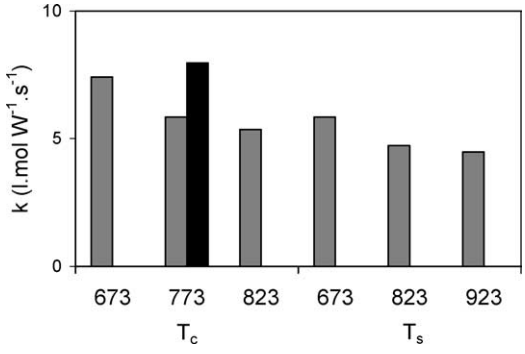

Fig. 10. Thiophene HDS activity of NiW/ASA as a function of the calcination temperature (T_C) and the sulfidation temperature (T_S). The effect of the calcination temperature was measured at a sulfidation temperature of 673 K, while the sulfidation temperature dependence was measured for materials calcined at 773 K. The sulfidation pressure (P_S) was kept at 1 bar (gray) except for one sample which was sulfided at 15 bar (black).

exchange reactions that proceed progressively up to 573 K. This corroborates with an almost constant contribution of a ^{57}Co:Ni(oxy)sulfide-type phase as probed by MES. One observes a small decrease of the QS of this phase which can be explained by a small degree of sintering. At a sulfidation temperature of 573 K the contribution of Ni–W–S-type phases becomes visible. Concomitantly, the W EXAFS data point to the start of tungsten sulfidation in NiW/ASA-673, although the structural parameters do not show the typical W–W coordination at a distance of 3.16 Å in WS_2. The appearance of a Mössbauer signal related to Ni–W–S structures is attributed to a redispersion of the small NiS_x particles over the edges of tungsten sulifde particles. This implies that these NiS_x species are mobile over the support surface. This phenomenon was earlier reported for NiW/γ-Al_2O_3 [2,12]. In this view, the interaction of mobile Ni-sulfide species with WS_2-like structures leads to formation of smaller NiS_x particles in Ni–W–S-type structures. A further increase of the sulfidation temperature to 673 K leads to more complete sulfidation of the tungsten phase and a further decrease of the NiS_x particle size as derived by the increase of the QS to 1.41 mm s^{-1}. At this sulfidation temperature, the W EXAFS data also show W–W coordinations typical for WS_2. This agrees with the idea that Ni-promoted WS_2 are structurally similar to Co–Mo–S structures [40] and hence are composed of highly dispersed Ni-sulfide clusters on the edges of WS_2. After sulfidation at 673 K, nickel is fully sulfided and equally distributed over two separate phases, i.e., (i) a phase consisting of very small particles on the edges of WS_2-like structures (Ni–W–S) and (ii) a phase consisting of small Ni-sulfide particles. Fig. 11 provides a schematic picture of the sulfidation of NiW/ASA. While in principle one expects a decrease of the QS value of the latter phase with temperature due to sintering of the bulk nickel sulfide phase—which was observed in the temperature range of 300–473 K—we find an increase in the quadrupole splitting of this phase at higher sulfidation temperatures. This small increase may suggest that there is some kind of interaction of these nickel sulfide species with a tungsten oxysulfide phase. Although not conclusive, this interpretation is underlined by the absence of a separate nickel sulfide phase from the TEM micrographs

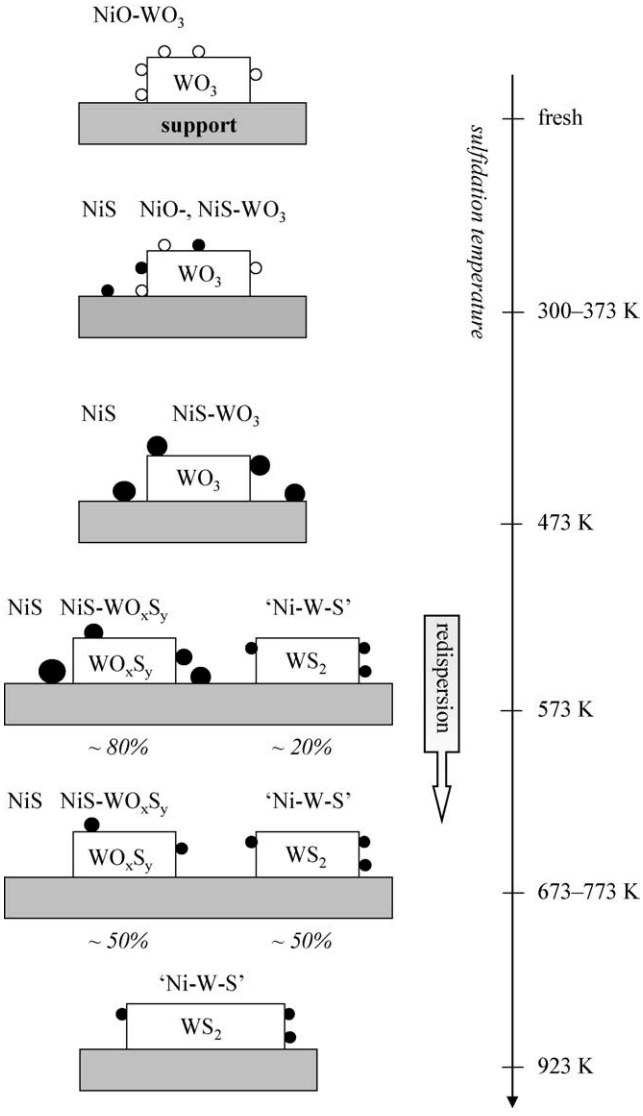

Fig. 11. Schematic representation of the sulfidation of supported NiW catalysts. Ni easily sulfides at low temperatures and probably interacts with a tungsten oxide phase. This latter phase transforms into an oxysulfidic phase (WO_xS_y). The nickel sulfide species eventually become smaller over this phase. Sulfidation to WS_2 probably proceeds already at 573 K to a small extent and is clearly observed after exposure to H_2S/H_2 at 673 K. Then, "Ni–W–S"-type structures are formed with very dispersed nickel sulfide clusters having a quadrupole splitting of 1.41 mm s^{-1}. The tungsten phase is fully sulfided at 923 K, the latter temperature inducing the growth of the WS_2 particles. Analysis of thiophene HDS data suggests that full crystallization of the WS_2 phase results in a lower intrinsic activity.

and the absence of Ni–Ni coordinations in NiW/ASA-673 (s 673). This view coheres with the suggestion of an interaction between nickel sulfide and WO_xS_y phases at relatively low sulfidation temperatures [10,12]. Although an optimum promoter concentration is found around Ni/W = 0.6 at./at., one observes a decrease in the thiophene HDS activity per mole Ni. This suggests that for higher Ni/W ratios nickel atoms end up in less active structures which may be dispersed nickel sulfide species located close to an oxysulfidic W phase. Further sulfidation will lead to a more completely sulfided WS_2 phase where the NiS_x clusters may disperse to very small or even mono-atomic Ni centers. This is relevant in the present case because the W EXAFS data show that W sulfidation is not complete at 673 K.

Although no intermediate W species is observed in the course of stepwise sulfidation for the sample calcined at 673 K, the structural parameters for NiW/ASA-823 (s 573) point to the presence of a WS_3-type phase next to the predominant WO_3 phase. Since the W phase is primarily located on the alumina part of the ASA support [7], a parallel can be drawn with W sulfidation in alumina-supported NiW. Reinhoudt et al. [41] deduced from TPS measurements that W sulfidation in NiW/Al_2O_3 calcined at 823 K proceeds via WS_3. It may thus well be that WS_3 is formed as an intermediate phase in the sulfidation from WO_3-type phases to WS_2. A WS_3 intermediate phase has also been found in the case of sulfidation of tetrathiotungstate [36], but not during the sulfidation of bulk WO_3 phases [6]. Although the latter precursor is the more relevant one for our case, one also must take into account that the support may strongly influence the mechanism of sulfidation. In the present work, we only found indications for WS_3 intermediates after single-step sulfidation at 573 K for NiW/ASA-823. In the other catalysts, we did not observe this intermediate phase at this sulfidation temperature. Most likely, the mode of sulfidation has some influence on the formation of the intermediate phases.

The influence of the sulfidation temperature on the morphology of the sulfide phases as derived from TEM micrographs is compared for NiW/ASA-673 (s 673) and (s 923). The average slab length for the sample sulfided at 673 K is 2.9 nm. The slabs are predominantly present as single-layered slabs. After increasing the sulfidation temperature to 923 K, the average slab length increases to 4.4 nm and a small decrease of the number of single-layered slabs is noted. Increasing the sulfidation temperature thus leads to a strong growth of the lateral dimensions of the WS_2 slabs and a small increase in stacking degree. The thiophene HDS performance for NiW/ASA-673 decreases strongly for higher sulfidation temperatures (Fig. 10). Although one expects that more complete W sulfidation leads to a higher gas-phase thiophene HDS performance, the decrease in dispersion of the WS_2 slabs appears to be of overriding importance. A comparison of the decrease in HDS performance ($\sim$ 40%) and in WS_2 dispersion ($\sim$ 30%) evaluated from the average fraction of W at the edges in Table 4 between NiW/ASA-673 (s 673) and (s 923) points to an additional effect of the crystallinity of the tungsten sulfide phase. Although the difference is relatively small, the decrease in HDS performance is larger than expected on the basis of the loss in dispersion. Moreover, we note that part of the tungsten phase is oxysulfidic after sulfidation at 673 K which negatively influences the activity. Kooyman et al. [20] have reported that fully sulfided, but distorted MoS_2 structures in $CoMo/Al_2O_3$ perform better in thiophene HDS than fully sulfided, better crystallized ones. The higher activity may be caused by the distortions present due to residual interactions

with the support surface, leading, for instance, to bending of the crystallites. Although the effect is smaller in the present case—possibly due to the fact that at a sulfidation temperature of 673 K the catalyst is partly oxysulfidic which results in a lower thiophene HDS activity—we can tentatively formulate that W-based catalysts exhibit a high thiophene HDS activity when the tungsten phase is fully sulfided but not yet fully crystallized. Formally, one should consider the active phase in NiW/ASA-673 (s 923) as a type II phase because in this case full sulfidation is obtained and all linkages with the support surface are broken. Similar to the study on Mo-based catalysts, it appears that the crystallinity of the WS_2 influences the HDS activity. One should then reconsider the definition of the type I/II formalism [44].

4.2. Influence of calcination temperature

The EXAFS FT function of NiW/ASA-773 (s 673, 15) exhibits considerably higher peak intensities than the FT function of NiW/ASA-823 (s 673, 15). This is reflected in the lower W–S and W–W coordination numbers in NiW/ASA-823. The rather low value for $N_{W–S}$ [4.8) is indicative for incomplete WS_2 formation and implies a partially oxidic tungsten phase. These oxygen atoms were not detected by W EXAFS. Apparently, the oxide atoms are not present at regular distances, which suggests that one is dealing with a kind of amorphous oxysulfide phase (WO_xS_y phase). In contrast to NiW/ASA-823 (s 673, 15), NiW/ASA-773 (s 673, 15) is sulfided more completely ($N_{W–S} = 6.1$). The lower W sulfidation degree resulting from a higher calcination temperature explains the decrease in thiophene HDS activity. Although the present data on the effect of sulfidation temperature are limited to samples sulfided at 15 bar, they correspond qualitatively to those found for NiW/Al_2O_3 [9–12] sulfided at atmospheric pressure. In those studies, calcination at higher temperatures also results in a lower activity in gas-phase thiophene HDS. We also investigated the influence of the calcination temperature on the morphology of the samples with TEM. The effect of increasing the calcination temperature from 673 to 773 K is twofold: the average slab length is lower (decreases from 2.9 to 2.6 nm) and the average stacking degree has increased from 1.1 to 1.4. The decrease in slab length is due to a larger number of particles of subnanometer size. Such particles were earlier observed by Reinhoudt et al. [9] in a TEM study of NiW/Al_2O_3 catalysts. Recently, similar species were reported in Mo-based catalysts [45]. Given that the WS_2 particles in sulfided NiW/ASA are primarily located on the Al_2O_3 part of the ASA support [7], we expect that similar phenomena occur for the present ASA-supported catalysts. The number of such subnanometer particles in the alumina case [9] was found to increase with the calcination temperature. More severe sulfidation conditions resulted in the lateral growth of these subnanometer particles to particles of 1–2 nm that were regarded as nuclei for the formation of WS_2 slabs. Reinhoudt et al. [9] suggested that the subnanometer particles containing Ni and W represented a partially sulfided intermediate species during sulfidation. Accordingly, the observed increase in density of subnanometer particles in NiW/ASA-773 can be attributed to a lower W sulfidation degree. This should be due to a lower W sulfidation degree at a higher calcination temperature which is in line with the present EXAFS fit results. The second effect of a higher calcination temperature is a slight increase in the stacking degree, possibly due to some mobility of tungstate in the oxidic precursor. This may lead to the migration of tungstate from the ASA patches to alumina parts of the support, where the binding with tungstate is preferred [7]. Although NiW/ASA-773 (s 673) exhibits a smaller particle size than NiW/ASA-673 (s 673), the higher W sulfidation degree of the latter catalysts leads to a significantly higher thiophene HDS activity. This agrees with the notion that the W sulfidation degree is a crucial parameter for the gas-phase thiophene HDS performance.

Fig. 3a clearly shows that NiW/ASA-773 (s 673, 15) exhibits more pronounced coordinations in the region of the second W–W contributions (6.32 and 6.41 Å) compared to NiW/ASA-823 (s 673, 15). The presence of coordination shells at such large distances is characteristic for long-range ordering of the WS_2 structure. Shimada et al. [46] similarly found more pronounced features for this coordination shell in the W EXAFS FT function of a NiW/Al_2O_3 catalyst that was used in second stage hydrotreating of coal-derived liquids. They attributed this to agglomeration of small WS_2 crystallites, especially in the lateral direction. Although this may also be valid in the present case, we did not observe an increase in the second W–W coordination shell for NiW/ASA-773 (s 673) after raising the sulfidation pressure from 1 to 15 bar, despite of a substantial larger average slab length observed by TEM. We conclude that next to the slab length also the crystallinity of the tungsten sulfide patches is important. Thus, a lower calcination temperature may result in a better crystallized WS_2 phase. Walton and Hibble [36] showed that even if WS_2 is poorly crystalline, this does not exclude the presence of a second W–W shell in the W EXAFS FT function. Differences in crystallinity between samples calcined at various calcination temperatures may thus be reflected in variations in the peak intensity of the second W–W shell.

4.3. Influence of sulfidation pressure

An increase of the sulfidation pressure from 1 to 15 bar has a marked positive effect on the activity of NiW/ASA-773 after sulfidation of 673 K. The catalyst sulfided at 15 bar exhibits stronger coordinations in the W EXAFS FT function (Fig. 3a). The resulting fit parameters (Table 2) indicate slightly higher W–S and W–W coordination numbers. Whereas the stacking degrees of both samples are similar (Table 4), sulfidation at 15 bar leads to higher average slab length of 3.4 nm as compared to 2.6 nm for the sample sulfided at atmospheric pressure. Moreover, the number of

subnanometer particles strongly reduces after more severe sulfidation. This can be understood in terms of progressive W sulfidation leading to the formation of a larger fraction of WS_2 slabs. The thiophene HDS data show a much higher performance ($\sim$ 140%) regardless of a small loss in dispersion ($\sim$ 20%), again stressing the important role of W sulfidation. Ramírez and Gutiérrez-Alejandre [47] found a relation between the average slab length and the sulfidation level of the W phase in NiW catalysts supported on Al_2O_3–TiO_2 mixed oxide and concluded that the growth of the particles did not originate from a sintering process but rather from a higher level of sulfidation of the W phase. Similarly, we conclude that the catalyst sulfided at 1 bar contains partially sulfided subnanometer particles with a lower W sulfidation degree compared to NiW/ASA-773 sulfided at a pressure of 15 bar. Although we could not perform Mössbauer measurements at elevated pressures, we surmise that further sulfidation of the W phase at elevated pressures results in a higher contribution of Ni–W–S-type structures. This would explain the higher thiophene HDS activity. These findings confirm previous reports [2,4,8–12] that stress the strong correlation between W sulfidation degree and gas-phase HDS activity.

From the slab lengths determined by TEM, we calculated the fraction of W atoms at the WS_2 edge surface assuming the slabs to be present as perfect hexagons. For these calculations the formulae of Kasztelan et al. [48] were applied. For the six W atoms at the corners of a perfect hexagonal slab $N_{W–W}$ equals 3, for the remaining edge atoms 4, while the W–W coordination of the atoms within the slab equals 6. For each observed slab the resulting average W–W coordination number was determined. These numbers were averaged over all the slabs in a particular sample. This procedure results in a W–W coordination number of 4.8 for NiW/ASA-773 sulfided at 1 bar and a value of 5.0 for NiW/ASA-773 sulfided at 15 bar. Conversely, the values for $N_{W–W}$ derived from the W EXAFS measurements are 3.6 and 4.0, respectively. Although the trends are similar, i.e., a higher W–W coordination number for the catalyst with the largest slabs, the values derived from TEM are higher than those derived from the EXAFS fit analysis. This discrepancy was earlier reported for the particle size determination of MoS_2 [20,49–51]. The limitation of TEM lies in the difficulty of differentiating the smallest particles from the structure of the alumina support. In principle, nevertheless, the applied magnifications should allow one to observe the smallest WS_2 (MoS_2) slabs with a size in the order of 10 Å. Shido and Prins discussed the limitations of EXAFS in determining particles sizes from the Mo–Mo coordination numbers [32] and developed a model in which distortions originating from surface relaxation were introduced through variations of the Mo–Mo distances in the MoS_2 crystallites. This study provides insight into the background of the lower coordination numbers observed from EXAFS as compared to TEM analysis. A function was proposed relating the EXAFS-derived Mo–Mo coordination number to the MoS_2 slab diameter. This led to a better agreement between the values determined from TEM and EXAFS analysis and provides some further clue that a careful TEM analysis produces an estimation of the MoS_2 dispersion. We applied this model to recalculate the W–W coordination numbers for our samples. The EXAFS coordination numbers were used to obtain a corrected value for the slab length. For NiW/ASA-773 sulfided at 1 bar, this results in a slab length of 26 Å in good agreement with the value derived from the TEM micrographs. A similar correction for the same sample sulfided at 15 bar gives a corrected slab length of 33 Å, again close to the TEM-derived value. Hence, we conclude that the distortions at the edges of the WS_2 slabs are the reason for the relatively low values of $N_{W–W}$ from the EXAFS measurements. For NiW/ASA-673 (s 923) the value of 5.3 for the W–W coordination would imply an average slab dimension of 120 Å which is much larger than the value of 45 Å determined by TEM. In this case, the original model of Kasztelan et al. [48] appears to produce a better value (ca. 40 Å). Taking into account the accuracy limits of N, an average slab length of 44 Å is not unreasonable. On the other hand, the incorrect prediction by the model by Shido and Prins in this particular case might relate to the fact that the WS_2 particles are better crystallized, rendering the surface relaxation correction unnecessary. This derives from the relatively high sulfidation temperature and corresponds well with the considerably larger particle size for this sample. As stated before, these differences in crystallinity may be an important parameter for the final HDS performance and have also been observed for MoS_2-based catalysts [20]. For NiW/ASA-673 (673), we also find deviations from the current model, i.e., a corrected slab length of 20 Å vs a value of 29 Å for NiW/ASA-673 (s 673). This may be partly due to the fact that the former sample is not fully sulfided with values of 2.8 and 4.4 for $N_{W–W}$ and $N_{W–S}$, respectively, but the difference may also relate to the single-step sulfidation of the latter sample which is known to produce a lower dispersion [52].

5. Conclusions

The effect of the sulfidation temperature, the sulfidation pressure, and the calcination temperature on the structure and thiophene hydrodesulfurization activity of ASA-supported NiW catalysts was studied by a combination of Mössbauer emission spectroscopy, W and Ni EXAFS, and TEM. Stepwise sulfidation Mössbauer measurements show that initially formed partially sulfided Ni particles redisperse upon sulfidation at about 573 K. This temperature coincides with the temperature where W sulfidation starts as derived from W L_{III} edge EXAFS measurements. ^{57}Co Mössbauer spectroscopy measurements clearly show that Ni–W–S-type structures are formed after sulfidation at 673 K. This observation tallies with the occurrence of a highly dispersed Ni-sulfide species and a WS_2-type phase derived from Ni and W EXAFS data. The remainder of the nickel sulfide phase

is probably present as dispersed nickel sulfide species in interaction with a oxysulfidic tungsten phase. Whereas CoMo and NiMo present on type of promoter ion on the edges of MoS_2, it appears that in sulfided NiW catalysts nickel can be present as very dispersed, probably atomically dispersed nickel species on the edges of WS_2 and as very small nickel sulfide species in close interaction with WO_xS_y-type phases. The sulfidation mechanism for ASA-supported NiW closely resembles that for alumina-supported NiW.

The calcination and sulfidation temperature have a pronounced effect on the development of the active phase and the resulting activity. The performance decreased after severe sulfidation at 923 K, which is explained by extensive sintering of the active phase providing fewer edges to render catalytically active Ni–W–S sites. Similar to Mo-based catalysts, a higher crystallinity of the active phase may suppress the thiophene HDS activity, although the conditions to achieve this for W-based catalysts are more severe. An increase of the calcination temperature (from 673 to 773 K) results in a distinct increase in the stacking degree of the WS_2 slabs (TEM) and the occurrence of a larger fraction of subnanometer particles that pertain to an oxysulfidic phase. This results in a lower performance in gas-phase thiophene HDS. On the other hand, an increase of the sulfidation pressure (from 1 to 15 bar) has a positive effect on the performance and can be attributed to a higher W sulfidation degree. The deviant values for the particle size as derived from TEM and EXAFS can be explained assuming distortions in the WS_2 slabs which render lower W–W coordination numbers than expected. For larger WS_2 crystallites inclusion of these distortions is not necessary, providing an additional indication that the small tungsten sulfide particles obtained after conventional sulfidation have a lower crystallinity than larger ones.

References

[1] W.R.A.M. Robinson, J.A.R. van Veen, V.H.J. de Beer, R.A. Santen, Fuel Proc. Technol. 61 (1999) 103.
[2] H.R. Reinhoudt, R. Troost, A.D. van Langeveld, S.T. Sie, J.A.R. van Veen, J.A. Moulijn, Fuel Proc. Technol. 61 (1999) 133.
[3] T. Kabe, Y. Aoyama, D. Wang, A. Ishihara, W. Qian, M. Hosoya, Q. Zhang, Appl. Catal. A 209 (2001) 237.
[4] M. Breysse, M. Cattenot, T. Décamp, R. Frety, C. Gachet, M. Lacroix, C. Leclercq, L. de Mourgues, J.L. Portefaix, M. Vrinat, M. Houari, J. Grimblot, S. Kasztelan, J.P. Bonnelle, S. Housni, J. Bachelier, J.C. Duchet, Catal. Today 4 (1988) 39.
[5] B. Scheffer, P.J. Mangnus, J.A. Moulijn, J. Catal. 121 (1990) 18.
[6] A.J. Van der Vlies, R. Prins, Th. Weber, J. Phys. Chem. B 106 (2002) 9277.
[7] M.J. Vissenberg, L.J.M. Joosten, M.E.H. Heffels, A.J. van Welsenes, V.H.J. de Beer, R.A. van Santen, J.A.R. van Veen, J. Phys. Chem. B 104 (2000) 8456.
[8] H.R. Reinhoudt, A.D. van Langeveld, R. Mariscal, V.H.J. de Beer, J.A.R. van Veen, S.T. Sie, J.A. Moulijn, Stud. Surf. Sci. Catal. 106 (1997) 263.
[9] H.R. Reinhoudt, A.D. van Langeveld, R.M. Stockmann, R. Prins, H.W. Zandbergen, J.A. Moulijn, J. Catal. 179 (1998) 443.
[10] H.R. Reinhoudt, E. Crezee, A.D. van Langeveld, P.J. Kooyman, J.A.R. van Veen, J.A. Moulijn, J. Catal. 196 (2000) 315.
[11] H.R. Reinhoudt, R. Troost, A.D. van Langeveld, J.A.R. van Veen, S.T. Sie, J.A. Moulijn, J. Catal. 203 (2001) 509.
[12] M.J. Vissenberg, Y. van der Meer, E.J.M. Hensen, V.H.J. de Beer, A.M. van der Kraan, R.A. van Santen, J.A.R. van Veen, J. Catal. 198 (2001) 151.
[13] L. Coulier, G. Kishan, J.A.R. van Veen, J.W. Niemantsverdriet, J. Phys. Chem. B 106 (2002) 5897.
[14] M. Sun, T. Bürgi, R. Cattaneo, A.D. van Langeveld, R. Prins, J. Catal. 201 (2001) 258.
[15] M. Sun, P.J. Kooyman, R. Prins, J. Catal. 206 (2002) 368.
[16] C.J. Song, C. Kwak, S.H. Moon, Catal. Today 74 (2002) 193.
[17] P. Atanasova, T. Tabakova, Ch. Vladov, T. Halachev, A. Lopez Agudo, Appl. Catal. A 161 (1997) 105.
[18] K.T. Ng, D.M. Hercules, J. Phys. Chem. 80 (1976) 2094.
[19] Y. van der Meer, M.J. Vissenberg, V.H.J. de Beer, J.A.R. van Veen, A.M. van der Kraan, Hyp. Interact. 139/140 (2002) 51.
[20] P.J. Kooyman, J.G. Buglass, H.R. Reinhoudt, A.D. van Langeveld, E.J.M. Hensen, H.W. Zandbergen, J.A.R. van Veen, J. Phys. Chem. B 106 (2002) 11795.
[21] M.W.J. Crajé, V.H.J. de Beer, A.M. van der Kraan, Catal. Today 10 (1991) 337.
[22] P.W. de Bont, M.J. Vissenberg, E. Boellaard, V.H.J. de Beer, J.A.R. van Veen, R.A. van Santen, A.M. van der Kraan, Hyp. Interact. 111 (1998) 39.
[23] US patent 3536604 (1968).
[24] A.M. van der Kraan, J.W. Niemantsverdriet, in: G.J. Long, J.G. Stevens (Eds.), Industrial Applications of the Mössbauer Effect, Plenum, New York, 1986, p. 609.
[25] F.W.H. Kampers, T.M.J. Maas, J. van Grondelle, P. Brinkgreve, D.C. Koningsberger, Rev. Sci. Instrum. 60 (1989) 2635.
[26] J.B.A.D. van Zon, D.C. Koningsberger, H.F.J. 't Blik, D.E. Sayers, J. Chem. Phys. 82 (1985) 5742.
[27] P.S. Kirlin, F.B.M. van Zon, D.C. Koningsberger, B.C. Gates, J. Phys. Chem. 94 (1990) 8439.
[28] B.K. Teo, P.A. Lee, J. Am. Chem. Soc. 101 (1979) 2815.
[29] S.I. Zabinsky, J.J. Rehr, A. Ankudinov, R.C. Albers, M.J. Eller, Phys. Rev. B 52 (1995) 2995.
[30] P.J. Kooyman, H.W. Zandbergen, A.D. van Langeveld, in: International Conference on Electron Microscopy, Mexico, ICEM 14, vol. 2, 1998, p. 491.
[31] M.W.J. Crajé, V.H.J. de Beer, J.A.R. van Veen, A.M. van der Kraan, in: M.L. Ocelli, R.R. Chianelli (Eds.), Hydrotreating Technology for Pollution Control, Dekker, New York, 1996, p. 95.
[32] M.W.J. Crajé, V.H.J. de Beer, A.M. van der Kraan, Bull. Soc. Chim. Belg. 100 (1991) 953.
[33] A. Balerna, E. Bernieri, E. Burattini, A. Kuzmin, A. Lusis, J. Purans, P. Cikmach, Nucl. Instrum. Methods A 308 (1991) 234.
[34] F. Hilbrig, H.E. Göbel, H. Knözinger, H. Schmelz, B. Lengeler, J. Phys. Chem. 95 (1991) 6973.
[35] T. Shido, R. Prins, J. Phys. Chem. B 102 (1998) 8426.
[36] R.I. Walton, S.J. Hibble, J. Mater. Chem. 9 (1999) 1347.
[37] A. Corrias, G. Mountjoy, G. Piccaluga, S. Sollinas, J. Phys. Chem. 103 (1999) 10081.
[38] R. Cattaneo, T. Shido, R. Prins, Stud. Surf. Sci. Catal. 127 (1999) 421.
[39] F.W. Lytle, R.B. Greegor, A. Panson, J. Phys. Rev. B 37 (1988) 1550.
[40] S.P.A. Louwers, M.W.J. Crajé, A.M. van der Kraan, C. Geantet, R. Prins, J. Catal. 144 (1993) 579.
[41] L.A. Grunes, Phys. Rev. B 27 (1983) 27111.
[42] S.P.A. Louwers, R. Prins, Jpn. J. Appl. Phys. 32 (1993) 457.
[43] T.I. Korányi, M. Dobrovolszky, T. Kotlai, K. Matusek, Z. Paál, P. Tétényi, Fuel Proc. Technol. 61 (1999) 55.
[44] E.J.M. Hensen, V.H.J. de Beer, J.A.R. van Veen, R.A. van Santen, Catal. Lett. 84 (2002) 59.
[45] P.J. Kooyman, E.J.M. Hensen, A.M. de Jong, J.W. Niemantsverdriet, J.A.R. van Veen, Catal. Lett. 74 (2001) 49.

[46] H. Shimada, N. Matsubayashi, M. Imamura, T. Sato, Y. Yoshimura, T. Kameoka, K. Masuda, A. Nishijima, Bull. Soc. Chim. Belg. 104 (1995) 353.
[47] J. Ramírez, A. Gutiérrez-Alejandre, Catal. Today 43 (1998) 123.
[48] S. Kasztelan, H. Toulhoat, J. Grimblot, J.P. Bonnelle, Appl. Catal. 13 (1984) 127.
[49] S. Eijsbouts, J.J.L. Heinerman, H.J.W. Elzerman, Appl. Catal. A 105 (1993) 53.
[50] C. Calais, N. Matsubayashi, C. Geantet, Y. Yoshimura, H. Shimada, A. Nisijima, M. Lacroix, M. Breysse, J. Catal. 174 (1998) 130.
[51] E.J.M. Hensen, P.J. Kooyman, Y. van der Meer, A.M. van der Kraan, V.H.J. de Beer, J.A.R. van Veen, R.A. van Santen, J. Catal. 199 (2001) 224.
[52] Y. van der Meer, PhD thesis, Delft University of Technology, Delft University Press, 2001, ISBN 90-407-2230-7.